

Gravitational wave background from neutron star phase transition

José Carlos N. de Araujo · Guilherme F. Marranghello.

Received: date / Accepted: date

Abstract We study the generation of a stochastic gravitational wave (GW) background produced by a population of neutron stars (NSs) which go over a hadron-quark phase transition in its inner shells. We obtain, for example, that the NS phase transition, in cold dark matter scenarios, could generate a stochastic GW background with a maximum amplitude of $h_{\text{BG}} \sim 10^{-24}$, in the frequency band $\nu_{\text{obs}} \simeq 20 - 2000$ Hz for stars forming at redshifts of up to $z \simeq 20$. We study the possibility of detection of this isotropic GW background by correlating signals of a pair of Advanced LIGO observatories.

Keywords Neutron Stars · Gravitational Waves · Strange Matter · Background

1 Introduction

The first scientific runs on the gravitational wave (GW) observatories have already been done and the first results have been obtained. In particular, we take the american interferometer LIGO that has already put some limits on the properties of neutron star (NS) ellipticities [1,2], for example. Putting some lower limits on such properties, like ellipticity, LIGO, among others like Virgo, GEO600 and TAMA, have contributed on the better understanding of NS properties.

NSs are excellent candidates to the first detection of GWs, with black holes (BHs), due to its great amount of matter constrained into a very small radius. NSs are astrophysical objects on which a great amount of quadrupole moment variation can be generated by a mountain on the star, a crust quake, a core quake, a glitch, rotation or collapse. All these events would generate and radiate GWs.

In this work, we address special attention to the GWs generated after a micro-collapse of the NS. Such event occurs, in a catastrophic way, when the NSs suffer a

J C N de Araujo
Instituto Espacial de Pesquisas Espaciais - Divisão de Astrofísica
Tel.: +55 12 39457223
Fax: +55 12 39456811
E-mail: jcarlos@das.inpe.br
G F Marranghello
Universidade Federal do Pampa

phase transition in its interior. This phase transition, in this work, is assumed by the releasing of quarks from the interior of hadrons. When the critical density is reached, quarks deconfine. As the quark matter equation of state is softer than the hadronic one, the NS shrinks.

It is widely accepted that NSs are born with fast rotating angular velocities. Due to magnetic torques, however, the NS periods could well be spun down. This spin-down causes a reduction in the centrifuge force and, consequently, the central energy density of the NSs increases. Those stars, born with densities close to that of the quark deconfinement, may undergo a phase transition forming a strange quark matter core. It is worth stressing, however, that it is not a common sense that such a transition really takes place.

As a consequence of such a putative phase transition, the stars could suffer a collapse which could excite mechanical oscillations. The great amount of energy generated in this process, $\Delta E \sim 10^{53} \text{ ergs}$ ($\sim 0.1 M_{\odot} c^2$) [3], could be dissipated, at least partially, in the form of GWs, which are studied in the present work.

The energy released to excite these mechanical oscillations can be driven into many different modes, such as the fundamental f-mode, the pressure p-mode, which are the overtones of the fundamental mode, g-modes, excited by a sharp difference in the density distribution, the w-mode, which is a pure relativity mode. The energy is also driven to heat the star, releasing neutrinos or ejecting the crust material [4].

The number of NSs that undergo a phase transition was estimated to be about $10^{-6} \text{ events/year/galaxy}$ [5]. However, this number depends on the properties of the phase transition and can increase (drop) to more (less) significant values. We investigate, in this work, the formation of a stochastic background of GWs originated by such event in scenarios of cosmological structure formation.

We have improved the calculation made by Sigl[6] by using a realistic equation of state for describing NS matter, previously studied with polytropic equations of state. For the rate of events, we have used the results obtained by Marranghello *et. al.*[5]. Finally, the amount of energy released in the GW mode is also estimated by realistic calculations made in ref.[7]. Moreover, we adopted in the present paper the history of star formation derived by [8], who employed hydrodynamic simulations of structure formation in a Λ cold dark matter (Λ CDM) cosmology. A larger set of variables, such as the initial mass function and progenitor masses, is also used for a richer analysis. Even though the results do not show great differences, once the physics included is more realistic, the model becomes more reliable.

Springel & Hernquist [8] obtain the history of star formation from hydrodynamic simulations of structure formation in Λ CDM cosmology. They study the history of cosmic star formation from the “dark ages”, at redshift $z \sim 20$, to the present. They take into account besides gravity and ordinary hydrodynamics, radiative heating and cooling of gas, supernova feedbacks, and galactic winds. Their paper improves previous studies which consider either semi-analytical models or numerical simulations.

It is worth mentioning that the story of star formation they obtain is consistent with observations. It is important to bear in mind, however, that nowadays observations give information from at most a redshift around $z \sim 5$. In the future, however, with the *Next Generation Space Telescope* (NGST) it will be possible to trace the cosmic star formation rate out to $z \geq 20$ (see, e.g., [9]).

Besides the reliable history of star formation by Springel & Hernquist, we consider the role of the parameters $\alpha_{i=1,2}$, which gives the fraction of the progenitor mass which forms the remnant NSs. We consider that the remnant mass is given as a function of

the progenitor mass $M_r = \alpha_1 m + \alpha_2$. Recall that a given initial mass function (IMF) refers to the distribution function of the stellar progenitor mass, and also to the masses of the remnant compact objects left as a result of the stellar evolution. In section 3 we show in detail why M_r is written as above.

In the present study we have adopted a stellar generation with a Salpeter IMF, which is consistent with Springel & Hernquist, since they show that population II stars could have been formed at high redshift too. We then discuss what conclusions would be drawn whether (or not) the stochastic background studied here is detected by the forthcoming GW observatories such as LIGO and VIRGO.

The paper is organized as follows. Section 2 deals with the NS equations of state adopted in our study; in Section 3 we consider the IMF and the NS masses; Section 4 deals with the GW production; in Section 5 we present the numerical results and discussions; in Section 6 the detectability of the background of GWs are considered and finally in Section 7 we present the conclusions.

2 Neutron stars and the nuclear matter equation of state

The global properties of mass and radius of compact stars are directly related to its equation of state. In the present study we do not adopt a polytropic equation of state, since this could result in a poor modeling. In particular, we consider a model developed by [10] for a new class of parameterized field-theoretical model described by a Lagrangian density where the whole baryon octet is coupled to scalar and vector fields through parameterized coupling constants.

The main characteristic of this model is to adjust these parameterized coupling constants to fit both the nuclear matter properties and the neutron stars observation data. Varying this parametrization, we are also able to fit the properties of some other field-theoretical models like the Walecka model and the Zimanyi-Moskowski model and compare our results to those of other relevant models in the literature as described by [10]. We are also able to reproduce calculations with higher and lower values for neutron star masses and radii, compression modulus and effective baryon masses.

Instead of performing the following calculations with a wide range of equations of state we preferred to describe our work choosing a representative equation of state whose coupling constants were chosen to be those that fit both the nuclear and stellar properties in an acceptable manner. It is important to notice that other parameterizations of this model could result in quite similar results, harder detection of the background or unreliable results due to the not well fitted characteristics of nuclear matter.

The nuclear matter Lagrangian density is described by

$$\begin{aligned} \mathcal{L} = & \sum_B \bar{\psi}_B \left(i\gamma_\mu (\partial^\mu - g_{\omega B}^* \omega^\mu) - (M_B - g_{\sigma B}^* \sigma) - \left[\frac{1}{2} g_{\rho B}^* \boldsymbol{\tau} \cdot \boldsymbol{\rho}^\mu \right] \right) \psi_B \\ & + \frac{1}{2} (\partial_\mu \sigma \partial^\mu \sigma - m_\sigma^2 \sigma^2) - \frac{1}{4} \omega_{\mu\nu} \omega^{\mu\nu} + \frac{1}{2} m_\omega^2 \omega_\mu \omega^\mu \\ & - \frac{1}{4} \boldsymbol{\rho}_{\mu\nu} \cdot \boldsymbol{\rho}^{\mu\nu} + \frac{1}{2} m_\rho^2 \boldsymbol{\rho}_\mu \cdot \boldsymbol{\rho}^\mu + \sum_l \bar{\psi}_l [i\gamma_\mu \partial^\mu - M_l] \psi_l, \end{aligned} \quad (1)$$

where the baryon field ψ_B is summed over the whole baryon octet and coupled to the scalar and vector fields σ , ω and ρ through the parameterized coupling constants $g_{\sigma B}^*$,

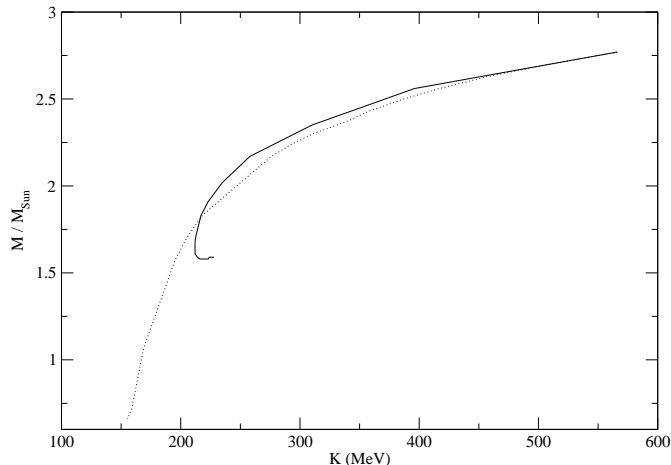


Fig. 1 The NS maximum masses versus the compression modulus, for different parametrization in the Taurines *et.al.* models. The solid line represents a parametrization in the scalar mesons while the dotted line describes a parametrization in both scalar and vector contributions of the nuclear force.

$g_{\omega B}^*$, $g_{\rho B}^*$. The free lepton fields ψ_λ contributes to the electrical equilibrium in the NS matter. The masses of the baryons, mesons and leptons are represented by M_B , $m_{\sigma,\omega,\rho}$ and m_λ , respectively. The free lepton fields contributes to the electrical equilibrium in the NS matter.

Using a parametrization for the baryon-meson coupling constants,

$$g_{\sigma}^* \bar{\psi} \sigma \psi = \frac{g_{\sigma} \sigma}{\left(1 + \frac{g_{\sigma} \sigma}{\lambda M}\right)^\lambda} \bar{\psi} \psi \quad (2)$$

this model describes a wide range of NS parameters, such as a maximum mass ranging from (very low values) $M = 0.66M_\odot$ up to $M = 2.77M_\odot$, and the corresponding radii that vary in the range of $8 < R < 13 \text{ km}$. Each pair in the mass-radius relation is associated with a different parametrization of the equation of state (see [10] for further details). Obviously, each value of such parametrization represents different values of nuclear matter properties.

The study of nuclear matter properties, however, is still a very open problem. A relevant parameter is the compression modulus, which defines the curvature of the equation of state or, in a few words, is related to the capability of matter to be compressed. One can see in Figure 1 that the maximum mass of NSs is obtained for large values of the compression modulus. The definition of K reads

$$K = 9 \left[\rho^2 \frac{d^2(\epsilon/\rho)}{d\rho^2} \right]_{\rho=\rho_0} \quad (3)$$

where ϵ is the energy density, ρ is the baryon density and ρ_0 the baryon saturation density. Actually, the acceptable values for the compression modulus are constrained to be in range $200 < K < 300 \text{ MeV}$ [11, 12].

An important constraint to the equation of state is to describe a family of NSs with a maximum mass greater than the value obtained by the most massive known pulsar. The PSR J0751+1807 has a mass $M = 2.1 \pm 0.2M_\odot$ [13]. This condition has

to be fulfilled by the set of parameters chosen to describe the NS model. This first condition already constrains the value of compression modulus to $K \geq 220 \text{ MeV}$ when this model is considered. Smaller values of K would lead to masses smaller than $1.9M_{\odot}$ disagreeing with the measures of PSR J0751+1807 mass.

It is worth mentioning that quite recently [14] reported the discovery of eight new millisecond pulsars in NGC 6440 and NGC 6441. In particular, they could determined the mass of the pulsar J1748-2021B (NGC 6440B), namely $M = 2.74 \pm 0.21M_{\odot}$. If the mass of this pulsar is really high, this would mean that the value of the compression modulus would be around 500 MeV . In other words, our model could describe, in an extreme limit of coupling constants, hybrid stars with that value of gravitational mass. However, it would lead to values of nuclear matter properties that are not in complete agreement with experiments.

Another scenario to be discussed concerns the strange quark star. The model used in this analysis is the MIT bag model [15]. The MIT bag model describes, as its own name suggests, that baryons are composed by three quarks confined inside a bag. The effects of pressure difference in the interior and exterior regions of the bag are summarized in the bag constant.

Even with considerable advances in the study of QCD (quantum chromo-dynamics) on the lattice, from where we expect the most reliable theoretical results and the consequent advances in collision experiments, the bag constant still presents a very wide range of possible values. In the same way, the perturbative constant, α_c , the one that represents the first order correction to the strong interaction forces between quarks, also represents an open issue.

Once the transition to quark-gluon matter occurs, the weak interaction processes for the quarks u , d and s

$$u + s \rightarrow d + u \quad (4)$$

and

$$d + u \rightarrow u + s \quad (5)$$

will take place, and a rapid transition occurs with a consequent gravitational micro-collapse. As a result, a huge amount of energy is dissipated, some in the form of GWs produced by quasi-normal modes excitation. The amount of energy released during the transition is calculated to be around 10^{53} erg according to ref.[3]. Only a small part of this energy is released in the form of GWs [7].

3 Initial mass function and the neutron star masses

The calculation of the GW background from NS phase transition requires the knowledge of the distribution function of stellar masses, the so called stellar initial mass function (IMF), $\phi(m)$. Here the Salpeter IMF is adopted, namely

$$\phi(m) = Am^{-(1+x)}, \quad (6)$$

where A is the normalization constant and $x = 1.30$ (our fiducial value). The normalization of the IMF is obtained through the relation

$$\int_{m_1}^{m_u} m\phi(m)dm = 1, \quad (7)$$

Table 1 The values of $\alpha_{i=1,2}$ which determines the fraction of the NS remnant.

α_1	1/32	1/50	1/17
$\alpha_2 (M_\odot)$	3/4	1.1	0.53

where we consider $m_1 = 0.1 M_\odot$ and $m_u = 125 M_\odot$. For further details we refer the reader to, e.g., [16].

It is worth mentioning that concerning the star formation at high redshift, the IMF could be biased toward high-mass stars, when compared to the solar neighborhood IMF, as a result of the absence of metals [17, 18].

On the other hand, in the study by Springel and Hernquist, besides a high-mass star formation, it is shown that the population II stars, whose IMF could well be of the Salpeter's type, could start forming around redshift 20 or higher.

In the present study we consider this population II studied by these authors. Then, for the standard IMF, the mass fraction of NSs produced as remnants of the stellar evolution is

$$f_{\text{NS}} = \int_{m_{\text{min}}}^{m_u} M_r \phi(m) dm, \quad (8)$$

where m_{min} is the minimum stellar mass capable of producing a NS at the end of its life, and M_r is the mass of the remnant NS. Stellar evolution calculations show that the minimal progenitor mass to form NSs is $m_{\text{min}} = 8M_\odot$, while the maximum progenitor mass is $m_{\text{max}} = 25 - 40M_\odot$ (see, e.g., [19]).

We do not intend to discuss in the present paper stellar evolution scenarios related to the formation of NSs. Many works can be found in the literature concerning the study of stellar evolution, supernova and NS formation [20]. However, we need to formulate a relation between the progenitor star mass m and the remnant NS mass M_r . For the remnant, M_r , we take

$$M_r = \alpha_1 m + \alpha_2,$$

where α_1 and α_2 are constants; the first one is dimensionless and the second one is given in solar masses. As the results for stellar evolution are not yet fully determined, we studied this parametrization in three different scenarios for the values of α_1 and α_2 which would represent the distribution of NS mass as function of the progenitor mass (see Table 1 and the following sections). For example, considering NSs formed from progenitors with $m = 20M_\odot$ we would have remnants with masses $M_r = 1.375M_\odot$, $1.5M_\odot$ and $2.7M_\odot$. These parameters describe sharper or softer distribution of NS masses around the standard value of mass $M = 1.4M_\odot$. Note that we are considering in the end that M_r is independent of the redshift.

With these considerations at hand, the mass fraction of NSs reads up to $f_{\text{NS}} = 10^{-2}$ for $x = 1.30$, while the fraction of NSs that undergoes a phase transition ($f_{\text{NS}}^{\text{pt}}$) can drop down to values $\ll 1$ (see, e.g., [5]).

To assess the role of possible IMF variations in our results, other values of x have also been considered. Besides the standard IMF, two others have been studied, namely, with $x = 0.3$ and $x = 1.85$, which yield approximately ten times and one-tenth of mass fraction of NSs of the standard IMF, respectively.

Table 2 Models description: mass function constants, $\alpha_{1,2}$, progenitor, m , and remnant, M , mass ranges, redshift, z , and the observed frequency, ν .

Model	α_1	α_2	$\Delta m(M_\odot)$	$\Delta M(M_\odot)$	Δz	$\Delta \nu(Hz)$
A	1/32	3/4	8.0-40.00	1.00-2.00	0-20	48-2000
B	1/32	3/4	14.4-16.32	1.20-1.26	0-50	31-1666
C	1/32	3/4	14.4-16.32	1.20-1.26	0-20	75-1666
D	1/32	3/4	20.8-22.72	1.40-1.46	0-20	65-1428
E	1/50	1.1	8.0-40.00	1.26-1.90	0-20	50-1587
F	1/50	1.1	15.0-18.00	1.40-1.46	0-20	65-1428
G	1/17	0.53	8.0-25.00	1.00-2.00	0-20	48-2000

In order to cover a wide number of parameters we present, in Table 2, the models considered in our study. In the first column appears the name of the model; in the second and third columns we present different combinations of the parameters α_1 and α_2 , which imply in different ways to calculate the NS remnant mass for a given IMF; in the fourth column the mass range of the progenitor star; in the fifth column the NS remnant mass; in the sixth column the NS redshift formation, and finally in the seventh column the observed frequency, which are obtained via the empirical formulae given in reference [21].

These parameters are directly related to the number of NSs that goes over the phase transition. According to the NS models obtained by realistic equations of state, only a fraction of them develops a core composed by deconfined quarks and gluons. When we set the mass range of the progenitor mass, we are also setting the mass of the remnant object. Stars with higher mass reach central densities that are high enough to develop the quark core, while smaller stars do not. The available energy for GW emission generated in the collapse process is also implicit in the mass of the remnant star. The more massive is the star, greater is its core and greater is the energy difference between the neutron and the hybrid star. We have found that stars with baryonic mass $M_b = 2M_\odot$ develops a core as large as $R = 7km$ and can generate as much as $3 \times 10^{53} erg$ of energy, while stars with baryonic mass $M_b = 1M_\odot$ develops a small core with $R = 1km$ and has ten times less energy available from the transition. As we do not know for sure the amount of this energy that is driven in each mode and in order to simplify our calculations we have adopted the standard medium value of $0.01M_\odot$ for the released energy.

4 Gravitational wave production

The GWs can be characterized by their dimensionless amplitude, h , and frequency, ν . The spectral energy density, the flux of GWs, received on Earth, F_ν , in $erg\ cm^{-2}s^{-1}Hz^{-1}$, is (see, e.g., [22,23]).

$$F_\nu = \frac{c^3 s_h \omega_{obs}^2}{16\pi G}, \quad (9)$$

where $\omega_{obs} = 2\pi\nu_{obs}$, with ν_{obs} the GW frequency (Hz) observed on Earth, c is the velocity of light, G is the gravitational constant and $\sqrt{s_h}$ is the strain amplitude of the GW in $Hz^{-1/2}$.

The stochastic GW background produced by NS phase transition would have a spectral density of the flux of GWs and strain amplitude also related to the above equation (9). Therefore, in the above equation the strain amplitude takes into account the star formation history occurring at the ‘first light’, just after the ‘dark age’ epoch. The strain amplitude at a given frequency, at the present time, is a contribution of NSs with different masses at different redshifts. Thus, the ensemble of NSs formed produces a background whose characteristic strain amplitude at the present time is $\sqrt{s_h}$.

On the other hand, the spectral density of the flux can be written as [24, 25]

$$F_\nu = \int_{z_{cf}}^{z_{ci}} \int_{m_{\min}}^{m_u} f_\nu(\nu_{\text{obs}}) dR_{\text{NS}}(m, z), \quad (10)$$

where $f_\nu(\nu_{\text{obs}})$ is the energy flux per unit of frequency (in $\text{erg cm}^{-2}\text{Hz}^{-1}$) produced by the formation of a unique NS and dR_{NS} is the differential rate of NSs formation.

The above equation takes into account the contribution of different masses that collapse to form NSs occurring between redshifts z_{ci} and z_{cf} (beginning and end of the star formation phase, respectively) that produce a signal at the same frequency ν_{obs} . On the other hand, we can write $f_\nu(\nu_{\text{obs}})$ [26] as

$$f_\nu(\nu_{\text{obs}}) = \frac{\pi c^3}{2G} h_{\text{NS}}^2, \quad (11)$$

where h_{NS} is the dimensionless amplitude produced by the NS micro-collapse of a given star with mass m that generates at the present time a signal with frequency ν_{obs} . Then, the resulting equation for the spectral density of the flux is

$$F_\nu = \frac{\pi c^3}{2G} \int h_{\text{NS}}^2 dR_{\text{NS}}. \quad (12)$$

From the above equations we obtain for the strain amplitude

$$s_h = \frac{1}{\nu_{\text{obs}}^2} \int h_{\text{NS}}^2 dR_{\text{NS}}. \quad (13)$$

Thus, the dimensionless amplitude reads

$$h_{\text{BG}}^2 = \frac{1}{\nu_{\text{obs}}^2} \int h_{\text{NS}}^2 dR_{\text{NS}}, \quad (14)$$

(see [27, 28]).

The micro-collapse produces GWs at frequency ν of the NS f-mode, and dimensionless amplitude given by [29]

$$h_{NS} \simeq 1 \times 10^{-19} \left(\frac{E}{M_\odot c^2} \right)^{1/2} \left(\frac{2kH z}{\nu} \right)^{1/2} \left(\frac{1Mpc}{d_L} \right) \quad (15)$$

where E is the available pulsation energy, and d_L is the luminosity distance to the source.

Recall that the energy available to excite the pulsating modes is directly related to the equation of state adopted.

Note that, since we are considering cosmological sources we have to take into account the redshift effect on the emission frequency, that is, a signal emitted at frequency ν_e at redshift z is observed at frequency $\nu_{\text{obs}} = \nu_e(1+z)^{-1}$.

For the differential rate of NS we consider only those that undergo micro-collapse, namely

$$dR_{\text{NS}} = \dot{\rho}_*(z) \frac{dV}{dz} f_{\text{NS}}^{\text{pt}} \phi(m) dm dz, \quad (16)$$

where $\dot{\rho}_*(z)$ is the star formation rate (SFR) density (in $\text{M}_\odot \text{yr}^{-1} \text{Mpc}^{-3}$), dV is the comoving volume element, and $f_{\text{NS}}^{\text{pt}}$, as already mentioned, is the fraction of NSs which may undergo a phase transition forming a strange quark matter core.

The comoving volume element is given by

$$dV = 4\pi \left(\frac{c}{H_0} \right) r_z^2 \mathcal{F}(\Omega_M, \Omega_\Lambda, z) dz, \quad (17)$$

with

$$\mathcal{F}(\Omega_M, \Omega_\Lambda, z) \equiv \frac{1}{\sqrt{(1+z)^2(1+\Omega_M z) - z(2+z)\Omega_\Lambda}}, \quad (18)$$

and the comoving distance, r_z , is

$$r_z = \frac{c}{H_0 \sqrt{|\Omega_k|}} S \left(\sqrt{|\Omega_k|} \int_0^z \frac{dz'}{\mathcal{F}(\Omega_M, \Omega_\Lambda, z')} \right), \quad (19)$$

where

$$\Omega_M = \Omega_{\text{DM}} + \Omega_{\text{B}} \quad \text{and} \quad 1 = \Omega_k + \Omega_M + \Omega_\Lambda \quad (20)$$

are the usual density parameters for the matter (M), i.e., dark matter (DM) plus baryonic matter (B), curvature (k) and cosmological constant (Λ). The function S is given by

$$S(x) = \begin{cases} \sin x & \text{if closed,} \\ x & \text{if flat,} \\ \sinh x & \text{if open.} \end{cases} \quad (21)$$

The comoving distance is related to the luminosity distance by

$$d_L = r_z(1+z). \quad (22)$$

The set of equations presented above can be used to find the dimensionless amplitude of the GW background produced from a population of NSs which goes over a hadron-quark phase transition in its inner shells as a function of the SFR density, and related to the ‘first light’ epoch.

For the SFR density, we adopt the one derived by Springel and Hernquist (see, [8] for details), namely

$$\dot{\rho}_*(z) = \dot{\rho}_m \frac{\beta \exp[\Delta(z - z_m)]}{\beta - \Delta + \Delta \exp[\beta(z - z_m)]}, \quad (23)$$

where $\Delta = 3/5$, $\beta = 14/15$, $z_m = 5.4$ marks a break redshift, and $\dot{\rho}_m = 0.15 \text{M}_\odot \text{yr}^{-1} \text{Mpc}^{-3}$ fixes the overall normalization.

It is worth mentioning that these authors employed hydrodynamic simulations of structure formation in a Λ CDM cosmology with the following parameters: $\Omega_M = 0.3$, $\Omega_\Lambda = 0.7$, Hubble constant $H_0 = 100 h \text{ km s}^{-1} \text{ Mpc}^{-1}$ with $h = 0.7$, $\Omega_{\text{B}} = 0.04$,

and a scale-invariant primordial power spectrum with index $n = 1$, normalized to the abundance of rich galaxy clusters at present day ($\sigma_8 = 0.9$).

Another relevant physical quantity associated with the GW background is the closure energy density per logarithmic frequency span, which is given by

$$\Omega_{\text{GW}} = \frac{1}{\rho_c} \frac{d\rho_{\text{GW}}}{d \log \nu_{\text{obs}}}. \quad (24)$$

The above equation can be rewritten as

$$\Omega_{\text{GW}} = \frac{\nu_{\text{obs}}}{c^3 \rho_c} F_\nu = \frac{4\pi^2}{3H_0^2} \nu_{\text{obs}}^2 h_{\text{BG}}^2. \quad (25)$$

In the next section we present the numerical results and discussions, which come mainly from the equation for h_{BG} .

5 NUMERICAL RESULTS AND DISCUSSIONS

In this section we present the numerical results of the putative GW background related to the NS phase transition.

The Eq. 15 is the main equation to calculate such a GW background, with the relevant ingredients given by Eqs. 16 – 24. Basically, to integrate Eq. 15 one needs to specify the cosmological model, the star formation rate density, etc. We refer the reader to Section 4 to see in detail how the various relevant ingredients are taken into account.

More explicitly, to obtain the spectrum of the background using Eq. 15 one takes a given ν_{obs} and perform integrations in the variables m and z , where the integration intervals are those of the models present in Table 2. This procedure is repeated for different ν_{obs} 's, whose values are taken from the frequency band also present in Table 2.

In Figure 2 we compare the background of GWs generated by NSs, which undergo phase transition, with that by the BH formation, which undergo quasi-normal mode instability (see [30] for details). In particular, for the NSs we consider two situations.

We consider in Figure 2 two versions of the model B (see Table 2): one with its original values, namely, $f_{\text{NS}}^{\text{pt}} \sim 0.01$ and the other one, just as an example, with $f_{\text{NS}}^{\text{pt}} = 1$. Obviously, even the most favorable values for nuclear and subnuclear matter coupling constants could not make $f_{\text{NS}}^{\text{pt}}$ even tend to 1, but this model is included just as a matter of comparison, as it would represent an upper limit. In both cases we consider $E \sim 0.01 M_\odot c^2$, which means that approximately only a tenth of the energy generated in phase transition goes to the pulsating mode. Note that we are considering an energy release in GW about ten times higher than [6]. Later on we comment on how this choice modifies our conclusions concerning the putative detectability of the background studied here.

Note that the background of GWs generated by the NSs would have an amplitude greater than that generated by the BHs only if a considerable fraction of the NSs formed undergo phase transition.

In Figure 3 we compare how different laws to calculate the NSs mass, the remnant mass, for a Salpeter IMF, modify the spectrum of the background of GWs generated. Note that there is no significantly difference in the background for the three cases considered.

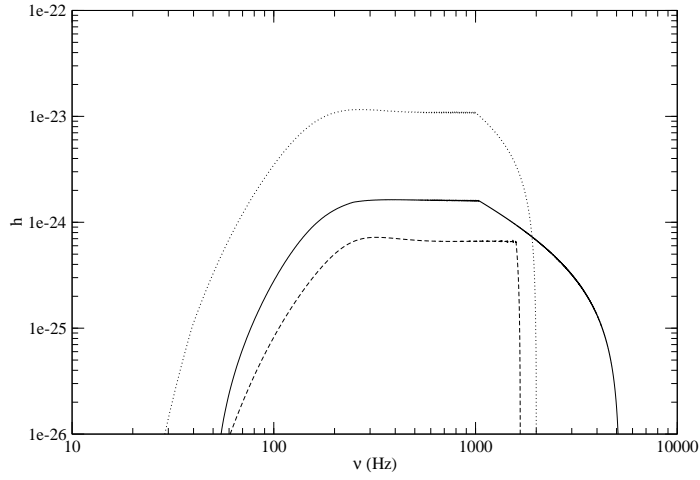


Fig. 2 The dimensionless amplitude for the GW background of stellar BH formation (solid line) and 1% of the NSs (dotted and dashed lines).

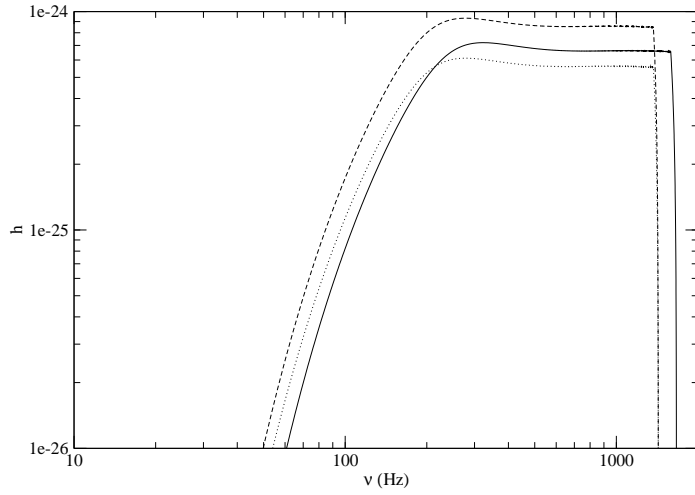


Fig. 3 The dimensionless amplitude for the GW background of micro-collapsed NSs for $1.2 < M < 1.26M_{\odot}$ (solid line), $1.4 < M < 1.46M_{\odot}$ (dotted line) and a sharper NS distribution with $1.4 < M < 1.46M_{\odot}$ (dashed line). We consider in these models $f_{\text{NS}}^{pt} = 0.01$ and $E = 0.01M_{\odot}c^2$.

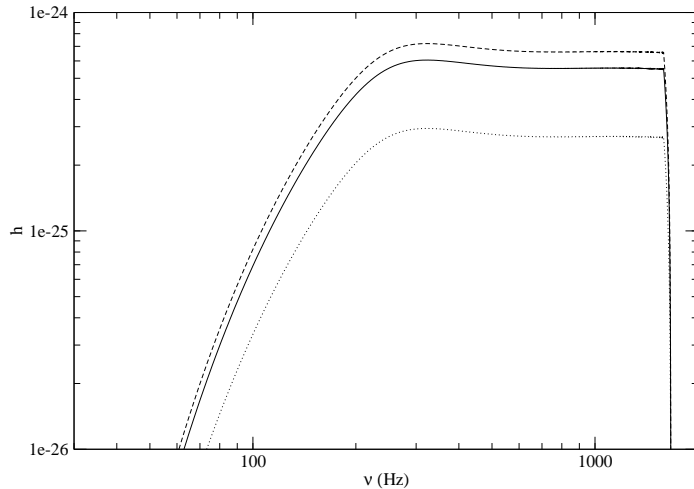


Fig. 4 The dimensionless amplitude for the GW background of micro-collapsed NSs for a IMF with $x = 1.30$ (solid line), 0.30 (dotted line) and 1.85 (dashed line). We consider in these models $f_{\text{NS}}^{pt} = 0.01$ and $E = 0.01 M_{\odot} c^2$.

We also investigated the role of the IMF in our results. In particular, besides the standard IMF ($x = 1.30$) we also consider two others, namely, $x = 0.30$ and 1.85 . This same choice was considered by [30] in their study on the background of GWs generated by the formation of population III stellar BHs. As with for the BHs the amount of NSs increases (decreases) for $x = 0.30$ (1.85) with respect to $x = 1.30$. In Figure 4 we compare these three cases. In this comparison, we consider model B.

We now compare model B, where we consider $f_{\text{NS}}^{pt} \sim 0.01$ and $E \sim 0.01 M_{\odot} c^2$, with the spectra of backgrounds of GWs for two other pulsating modes, considering these two very parameters. In particular, we present in Figure 5 the GW background of micro-collapsed NSs considering the contributions of the p-mode at 6 kHz (dotted line) and the w-mode at 12 kHz (dashed line). As expected, see Figure 5, the higher the frequency is, the more the spectrum is shifted to the higher frequencies. Concerning the amplitude, the spectra do not present considerable differences among them.

It is worth mentioning that we did not take into account the g-mode in our calculations because the amount of energy put into this mode, which is related to density discontinuities [4], is much smaller than in the case of f- and p-modes and the frequencies related to this mode lie in a lower range of the spectrum.

A relevant question is whether the background we study here is continuous or not. The duty cycle indicates if the collective effect of the bursts of GWs generated during the collapse of a progenitor star generates a continuous background. The duty cycle is defined as follows:

$$DC = \int_{z_{cf}}^{z_{ci}} dR_{\text{NS}} \Delta \tau_{\text{GW}}^{-} (1+z), \quad (26)$$

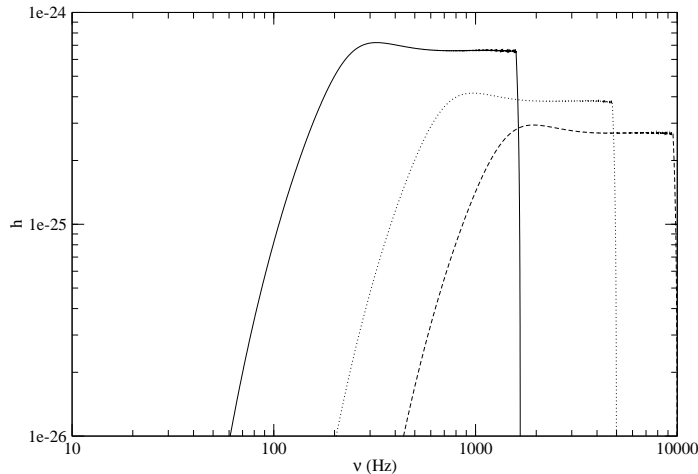


Fig. 5 The dimensionless amplitude for the GW background of micro-collapsed NSs considering the contributions of different quasi-normal modes. The f-mode (solid line), the p-mode at 6kHz (dotted line) and the w-mode at 12kHz (dashed line). We adopted model B (f-mode) with $f_{\text{NS}}^{\text{pt}} = 0.01$ and $E = 0.01M_{\odot}c^2$. For the p- and w- modes we also considered for comparison these very two parameters.

where $\Delta\tau_{\text{GW}}^{-}$ is the average time duration of single bursts at the emission, which amounts to ~ 100 ms to the f-mode of NSs, as obtained through the empirical equations of ref.[21]. This value for the f-mode damping time is quite different from that adopted by Sigl [6], who assumed a value of $1/3$ ms.

Since the star formation rate could be high, a significant amount of GWs could be produced. We also note that, independently of the primordial cloud mass and of the redshift of collapse, star formation occurring at high redshift could produce high duty cycle values, which lead us to conclude that the stochastic GW background could be continuous. For all the models studied here the duty cycle is > 1 .

In the next section we consider the detectability of the background of the GW background that we propose exists.

6 DETECTABILITY OF THE BACKGROUND OF GRAVITATIONAL WAVES

The background predicted in the present study cannot be detected by single interferometric detectors, such as VIRGO and LIGO (even by the forthcoming advanced ones). However, it is possible to correlate the signal of two or more detectors to detect the background that we propose exists. Christensen [31] was the first to show that this kind of signal can, in principle, be detected by correlating the outputs of two different detectors. However, the main requirement that must be fulfilled is that they must have independent noise. This study was improved by [32] and by [33]. The reader should also refer to the papers by [34] and [35] who also deal in detail with such an issue.

Table 3 For the models of Table 2 with different values of f_{NS}^{pt} , we present the S/N for pairs of Initial, Enhanced and Advanced LIGO observatories for one year of observation. We consider in the calculations $E = 0.01M_{\odot}c^2$.

Model	f_{NS}^{pt}	S/N		
		Initial LIGO	Enhanced LIGO	Advanced LIGO
A	1.0	8.6×10^{-4}	2.0×10^{-3}	2.4×10^{-1}
B	0.01	2.2×10^{-6}	4.8×10^{-6}	2.0×10^{-4}
C	0.01	2.2×10^{-6}	4.8×10^{-6}	2.0×10^{-4}
D	0.01	2.8×10^{-6}	6.3×10^{-6}	2.6×10^{-4}
E	1.0	1.1×10^{-4}	1.5×10^{-3}	3.0×10^{-2}
F	1.0	5.6×10^{-6}	1.0×10^{-5}	5.7×10^{-4}
G	1.0	6.5×10^{-4}	1.5×10^{-3}	7.6×10^{-2}

To assess the detectability of a GW signal, one must evaluate the signal-to-noise ratio (S/N), which for a pair of interferometers is given by (see, e.g., [33,34])

$$(S/N)^2 = \left[\left(\frac{9H_0^4}{50\pi^4} \right) T \int_0^{\infty} d\nu \frac{\gamma^2(\nu) \Omega_{GW}^2(\nu)}{\nu^6 S_h^{(1)}(\nu) S_h^{(2)}(\nu)} \right] \quad (27)$$

where $S_h^{(i)}$ is the spectral noise density, T is the integration time and $\gamma(\nu)$ is the overlap reduction function, which depends on the relative positions and orientations of the two interferometers. For the $\gamma(\nu)$ function we refer the reader to [33], who was the first to calculate a closed form for the LIGO observatories. Flanagan [33] (see also [34]) showed that the best window for detecting a signal is $0 < \nu < 64$ Hz, where the overlap reduction function has the greatest magnitude.

Here we consider, in particular, the LIGO interferometers: the Initial, the Enhanced and the Advanced ones. For the Initial LIGO, the present configuration, the sensitivity curve has been taken from http://www.ligo.caltech.edu/~jzweizig/distribution/LSC_Data/. It is worth mentioning that the design-sensitivity curve was almost attained by the S5 run. For the Enhanced LIGO, which is an upgrade of the Initial LIGO and to be operative briefly, the sensitivity curve has been taken from <http://www.ligo.caltech.edu/docs/T/T060156-01.pdf>, in particular from its Fig. 12. The Enhanced LIGO is approximately a factor of two more sensitive than the Initial LIGO. Finally, for the Advanced LIGO, designed to be approximately a factor of ten more sensitive than the Initial LIGO, the sensitivity curve has been taken from http://lhocds.ligo-wa.caltech.edu:8000/advligo/LSC_Modeling?action=AttachFile&do=get&target=iscddFeb19.pdf, in particular from its Fig. 1.

We show in Table 3 the S/N for the models of Table 2 for the three different LIGO generations and for different values of f_{NS}^{pt} .

As shown in Table 3, the signal-to-noise ratio for all models studied is lower than one, even for an advanced LIGO. Therefore, contrary to the claim of [6] such a putative GW background would hardly be detected.

Using the same parameters of model B with $f_{NS}^{pt} = 0.01$ and $E = 0.01M_{\odot}c^2$, we have also investigated the role of the variations in the IMF modifying the exponent x . We have found, for the Advanced LIGO, a signal-to-noise ratio of 3.4×10^{-5} , for $x = 0.30$, and 1.5×10^{-4} , for $x = 1.85$. As before, the signal-to-noise ratios are lower than 1.

We still have to mention the results for different frequencies, which correspond to the excitation of p- and w-modes. From our calculations, with the same parameters shown for model B, i.e., with $f_{\text{NS}}^{\text{pt}} = 0.01$ and $E = 0.01 M_{\odot} c^2$, we have changed the frequencies to $\nu_e = 3, 6$ and 12 kHz, we obtain a signal-to-noise ratio for Advanced LIGO equal to 2.8×10^{-5} , 7.8×10^{-6} and 1.3×10^{-8} , respectively. These results show that such background would not either be detected.

Note that the signal-to-noise ratio, for given IMF, α_i , and integration time, depends on $f_{\text{NS}}^{\text{pt}}$ and E as follows

$$(S/N) \propto f_{\text{NS}}^{\text{pt}} E; \quad (28)$$

and it also depends on the SFR density in a more complicated way, namely, through an integral involving the redshift z . The higher the star formation rate, the higher the signal-to noise ratio will be.

Just as a matter of comparison, even considering models with $f_{\text{NS}}^{\text{pt}} = 1$, a signal-to-noise ratio significantly greater than one for the Advanced LIGO would be possible either the SFR density would be much greater than that by Springel & Hernquist, or the energy generated in the phase transition were almost completely channeled to excite the f- mode. Obviously, an optimistic combination of the SFR density and the energy channeled to the f-mode would also render the same.

Still concerning the energy release in GWs, the above equation shows explicitly how the detectability is affected for lower values of E . For example, adopting an energy release as that by [6] the signal-to-noise ratios presented in Table 3 would be ten times lower.

7 CONCLUSIONS

We present here a study concerning the generation of GWs produced from a cosmological population of NSs. These stars may undergo a phase transition if born close to the transition density, suffering a micro-collapse and exciting quasi-normal modes.

This work differs from the previous one done by Sigl in two essential points. First, we have calculated the NS star structure using realistic equation of state, instead of a polytropic model, obtained through a field-theoretical model which takes into account the microstructure of matter composed by the whole baryon octet, coupled to meson fields. We have also taken into account, into the quark sector, the standard MIT bag model. The transition is constructed via Gibbs criteria. We have calculated the amount of energy released by the transition and the rate of stars that undergo this microcollapse. Second, we have used another scenario for the cosmical star formation rate. We also have made a study considering various scenarios varying the set of parameters that gives the main characteristics of star formation masses, etc.

We show that a detectable background is possible only if the SFR density is much greater than that predicted by Springel & Hernquist or if the energy generated in the phase transition is almost completely channeled to excite the f- mode. Obviously, a too optimistic combination of these two possibilities could do the same.

It is worth mentioning that even planned detectors like DECIGO and BBO would not be sufficiently sensitive to detect the background considered here.

Finally, it is worth mentioning that Sigl claims a putative marginal detection if the majority of NSs undergo a phase transition. In our study we obtain a similar

conclusion for some of our models if the above condition is fulfilled ($f_{\text{NS}}^{pt} = 1$) and for an integration time significantly larger than one year.

One could ask why we obtained such a conclusion even adopting a release of GW energy larger than that adopted by Sigl. One reason for that is related to the SFR densities we adopted, namely, in his case a larger number of NSs is generated. As a matter of comparison, if you multiplied the SFR density by a factor of ten the signal-to-noise ratio would be multiplied by this very factor. Other reasons could be related to the way we calculate the NSs remnants (see Table 3) and the value Sigl adopted for the damping time. A damping time of ~ 100 ms instead of one of $1/3$ ms could modify his results significantly.

Acknowledgments

GFM and JCNA would like to thank CNPq (grants 381682/2006-4 and 307424/2007-3, respectively) for financial support. The authors would like also to thank the referees for useful suggestions and criticisms. In particular, we would like to thank one of the referees who called our attention to the correct LIGO nomenclature as well as for kindly sent us the updated LIGO'S sensitivity curves.

References

1. Owen, B. J., Phys. Rev. Lett, 95, 211101 (2005).
2. Haskell, B., Andersson, N., Jones, D. I. & Samuelsson, L., Phys. Rev. Lett, 99, 231101 (2007)
3. Marranghello, G. F., Vasconcellos, C. A. Z. & de Freitas Pacheco, J. A., Phys. Rev., D66, 064027 (2002).
4. Miniutti, G., Pons, J. A., Berti, E., Gualtieri L., Ferrari V., Mon. Not. Roy. Ast. Soc. 338,389 (2003)
5. Marranghello, G. F., Regimbau, T. & de Freitas Pacheco, J. A., Int. J. Mod. Phys., D16, 313 (2007).
6. Sigl, G., J. Cosm. Astrop. Phys., 04, 002 (2006).
7. Marranghello, G. F., Int. J. Mod. Phys., D16, 333 (2007).
8. Springel, V. & Hernquist, L., Mon. Not. Roy. Ast. Soc., 339, 312 (2003).
9. Mackey, J., Bromm, V. & Hernquist, L., Astrophys. J., 586, 1 (2003).
10. Taurines, A. R., Vasconcellos, C. A. Z., Malheiro, M. & Chiapparini, M., Phys. Rev., 63, 065801 (2001).
11. Blaizot, J. P., Phys. Rept., 64, 171 (1980).
12. Myers, W. D. & Swiatecki, W. J., Nucl. Phys., A601, 141 (1996).
13. Nice, D. J. et al., Astrophys. J., 634, 1242 (2005).
14. Freire, P. C. C., Ransom, S. M., Bgin, S., Stairs, I. H., Hessels, J. W. T., Frey, L. H. & Camilo, F., Astrophys. J., 675, 670 (2008).
15. Chodos, A., Jaffe, R. L., Johnson, K., Thorne, C. B. & Weiskopf, V. F., Phys. Rev., D9, 3471 (1974)
16. de Araujo, J. C. N., Miranda. O. D. & Aguiar, O. D., Mon. Not. Roy. Ast. Soc., 330, 651 (2004).
17. Bromm, V., Coppi, P. S. & Larson, R. B., Astrophys. J. Lett., 527, L5 (1999)
18. Bromm, V., Coppi, P. S. & Larson, R. B., Astrophys. J., 564, 23 (2002).
19. Timmes F. X., Woosley S. E., Weaver T. A., Astrophys. J. Supl., 98, 617 (1995).
20. Janka H.-Th., Marek A., Mueller B., Scheck L. astro-ph/07123070. To be published in the proceeding of the conference 40 years of pulsars: millisecond pulsars, magnetars and more.
21. Benhar O., Ferrari V., Gualtieri L., Phys. Rev., D70, 124015 (2004).
22. Douglass, D. H. & Braginsky, V. G. 1979 in *S.W. Hawking, W. Israel*, eds., General Relativity: An E
23. Hils, D., Bender, P. L., Webbink, R. F., Astrophys. J., 360, 75 (1990).

-
24. Ferrari, V., Matarrese, S. & Schneider, R., *Mon. Not. Roy. Ast. Soc.*, 303, 247 (1999).
 25. Ferrari, V., Matarrese, S. & Schneider, R., *Mon. Not. Roy. Ast. Soc.*, 303, 258 (1999).
 26. Carr, B. J., *Astron. & Astrophys.*, 89, 6 (1980).
 27. de Araujo, J. C. N., Miranda, O. D. & Aguiar, O. D., *Phys. Rev.*, D61, 124015 (2000).
 28. de Araujo, J. C. N., Miranda, O. D. & Aguiar, O. D., *Class. Quant. Grav.*, 22, S471 (2005).
 29. Andersson, N. & Kokkotas, K. D., *Mon. Not. Roy. Ast. Soc.*, 299, 1059 (1998).
 30. de Araujo, J. C. N., Miranda, O. D. & Aguiar, O. D., *Mon. Not. Roy. Ast. Soc.*, 348, 1373 (2004).
 31. Michelson, P. F., *Mon. Not. Roy. Ast. Soc.*, 227, 933 (1987).
 32. Christensen, N., *Phys. Rev.*, D46, 5250 (1992).
 33. Flanagan, E. E., *Phys. Rev.*, D48, 2389 (1993).
 34. Allen, B. 1997 in *J.-P. Lasota, J.-A. Mark, eds., Relativistic Gravitation and Gravitational Radiation*. Cambridge University Press, Cambridge, p. 373
 35. Allen, B. & Romano, J. D. *Phys. Rev.* D59, 102001 (1999).
 36. Owen, B. J., Lindblom, L., Cutler, C., Schutz, B. F., Vecchio, A. & Andersson, N., *Phys. Rev.*, D58, 084020 (1998).